Developmental Cell
Article

The NF-κB Signaling Protein Bcl10 Regulates Actin Dynamics by Controlling AP1 and OCRL-Bearing Vesicles

Sabrina Marion,[1,2,3] Julie Mazzolini,[1,2,3,9] Floriane Herit,[1,2,3,9] Pierre Bourdoncle,[1,2,3] Nadège Kambou-Pene,[1,2,3] Stephan Hailfinger,[4] Martin Sachse,[5] Jürgen Ruland,[6] Alexandre Benmerah,[1,2,3] Arnaud Echard,[7,8] Margot Thome,[4] and Florence Niedergang[1,2,3,*]

[1]Inserm, U1016, Institut Cochin, Paris, France
[2]CNRS, UMR 8104, Paris, France
[3]Université Paris Descartes, Sorbonne Paris Cité, Paris, France
[4]Department of Biochemistry, University of Lausanne, CH-1066 Epalinges, Switzerland
[5]Institut Pasteur, Imagopole, Plate-Forme de microscopie ultrastructurale, 25-28 rue du Dr Roux, 75724 Paris Cedex 15, France
[6]Institut für Klinische Chemie und Pathobiochemie, Klinikum rechts der Isar, Technische Universität München, 81675 München, Germany
[7]Institut Pasteur, Membrane Traffic and Cell Division Lab, 25-28 rue du Dr Roux, 75724 Paris Cedex 15, France
[8]CNRS, URA2582, Paris, France
[9]These authors contributed equally to the work
*Correspondence: florence.niedergang@inserm.fr
http://dx.doi.org/10.1016/j.devcel.2012.09.021

SUMMARY

The protein Bcl10 contributes to adaptive and innate immunity through the assembly of a signaling complex that plays a key role in antigen receptor and FcR-induced NF-κB activation. Here we demonstrate that Bcl10 has an NF-κB-independent role in actin and membrane remodeling downstream of FcR in human macrophages. Depletion of Bcl10 impaired Rac1 and PI3K activation and led to an abortive phagocytic cup rich in PI(4,5)P_2, Cdc42, and F-actin, which could be rescued with low doses of F-actin depolymerizing drugs. Unexpectedly, we found Bcl10 in a complex with the clathrin adaptors AP1 and EpsinR. In particular, Bcl10 was required to locally deliver the vesicular OCRL phosphatase that regulates PI(4,5)P_2 and F-actin turnover, both crucial for the completion of phagosome closure. Thus, we identify Bcl10 as an early coordinator of NF-κB-mediated immune response with endosomal trafficking and signaling to F-actin remodeling.

INTRODUCTION

The protein B cell lymphoma/leukemia-10 (Bcl10) plays a central role in the stimulation of immune responses triggered by immune recognition receptors, such as the B and T cell antigen receptors, as well as phagocytic receptors that bind to the Fc portion of immunoglobulins (FcRs) (Rawlings et al., 2006; Thome and Weil, 2007). Indeed, Bcl10-deficient mice are severely immunodeficient because of impaired antigen (Ag) receptor- and FcR-induced NF-κB activation and cytokine production (Chen et al., 2007; Klemm et al., 2006; Ruland et al., 2001; Xue et al., 2003). Bcl10 and its interaction partners Malt1 (MALT lymphoma translocation protein-1) and Carma1 (CARD-containing MAGUK protein-1) are essential signaling components in Ag receptor-triggered lymphocytes but also in cells derived from the activated B cell subtype of diffuse large B cell lymphomas (ABC-DLBCL), which critically depend on abnormal constitutive NF-κB activation for survival (Ngo et al., 2006). The appearance of lymphomas of the mucosa-associated lymphoid tissue (MALT lymphomas) often correlates with a persistent stimulation of the immune system by an infectious agent, such as *Helicobacter pylori* (Du, 2007). Aggressive forms of MALT lymphomas are characterized by chromosomal translocations of the genes encoding Bcl10 or Malt1, which are also thought to promote cellular proliferation by constitutive NF-κB activation (Du, 2007). Despite these recent insights into the biological relevance of Bcl10, the molecular function of Bcl10 is still poorly understood. Biochemical studies that were performed mainly in T cells have shown that Ag receptor stimulation triggers the recruitment and activation of Carma1 (also known as CARD11), which stimulates the subsequent recruitment of preformed Bcl10-Malt1 complexes. The assembled Carma1-Bcl10-Malt1 (CBM) complex activates NF-κB by promoting the physical recruitment and activation of the NF-κB-regulating IκB kinase (IKK) complex (Thome et al., 2010). The IKKβ kinase subunit phosphorylates IκBα, targeting it for ubiquitinylation and degradation by the proteasome. Freed NF-κB dimers (predominantly p65 (RelA)/p50) then translocate to the nucleus to activate gene transcription (Häcker and Karin, 2006). A related CBM complex containing the Carma1 homolog CARD9, Bcl10, and Malt1 is thought to play a similar role in promoting NF-κB activation by Dectin-1, Dectin-2, and FcR in monocytes/macrophages and dendritic cells (Bi et al., 2010; Gross et al., 2006; Hara et al., 2007). Myeloïd cells have a high expression of CARD9, which binds to Bcl10 via its CARD motif (Gross et al., 2006; Hara et al., 2008; Hara and Saito, 2009). During both fungal and bacterial internalization, CARD9 is actively recruited to phagosomes and required for efficient pathogen killing but not necessary for the entry process itself (Goodridge et al., 2009; Strasser et al., 2012; Wu et al., 2009). In contrast, we have previously shown that Bcl10 is required

for efficient entry of particles downstream of FcR signaling in human monocytes (Rueda et al., 2007). Upon TCR and FcR stimulation, silencing of Bcl10 impaired actin cytoskeleton reorganization required for immune synapse and phagocytic cup formation, respectively. However, the molecular mechanisms involved were not identified.

Phagocytosis strictly requires actin polymerization that, in the case of FcR, is driven by the small GTPases Rac1, Rac2, and Cdc42. Downstream effectors, such as the Wiskott-Aldrich syndrome protein (WASP) activate the Actin-Related Protein 2/3 complex (Arp2/3), which nucleates actin filaments. Phosphatidylinositol-4,5-bisphosphate ($PI(4,5)P_2$) is essential for the initial polymerization that drives pseudopod formation, and its conversion to $PI(3,4,5)P_3$ is required for pseudopod extension and phagosomal closure (Flannagan et al., 2012; Swanson, 2008). In addition, efficient phagocytosis relies on focal exocytosis of intracellular compartments that are thought to contribute to the release of membrane tension, allowing efficient phagosome formation around large particles (Braun and Niedergang, 2006; Swanson, 2008). Although the major part of the membrane forming a phagosome is of plasmalemmal origin (Touret et al., 2005), several intracellular compartments, including recycling endosomes containing the SNARE protein VAMP3/Cellubrevin (Bajno et al., 2000; Niedergang et al., 2003) and a subpopulation of late endosomes bearing the SNARE protein VAMP7/TI-VAMP (Braun et al., 2004), have been shown to be recruited and undergo focal exocytosis at the site of phagocytosis. In addition, we have shown that the clathrin-associated adaptor complex AP1 plays an important role in organizing focal exocytosis under the control of the ADP-ribosylation factor ARF1 (Braun et al., 2007).

In this study, we unraveled an unexpected function for the NF-κB signaling protein Bcl10 in promoting phagocytic cup extension and closure. Our data indicate that Bcl10 modulates Rac1 activity and PI3K activation and controls the delivery of AP1/EpsinR-positive vesicular compartments containing the $PI(4,5)P_2$ phosphatase oculocerebrorenal syndrome of Lowe 1 (OCRL1) in nascent phagosomes, thereby regulating F-actin dynamics. In addition, Bcl10 was required for the local recruitment and activation of NF-κB to the nascent phagosome. Thus, Bcl10 plays a crucial role in coordinating the activation of the NF-κB-mediated immune response and local signaling events regulating actin and membrane remodeling at the site of phagocytosis.

RESULTS

Bcl10 Controls Phagocytic Cup Extension and Closure

To better characterize the defect in phagocytosis observed after depletion of Bcl10 (Rueda et al., 2007), we generated THP1 human monocytic cells stably transduced with two distinct shRNA constructs directed against Bcl10 (Bcl10 KD). Cells transduced with a nonrelevant shRNA were used as control (Ctrl). Both shRNAs efficiently reduced Bcl10 expression, whereas the expression of the two other CBM proteins, Malt1 and CARD9, was not affected (Figure 1A). We also generated two stable THP1 cell lines overexpressing FLAG-tagged versions of either the wild-type Bcl10 protein (FLAG-Bcl10) or the Bcl10 serine 138 phosphorylation-deficient mutant (FLAG-S138A) (Rueda et al., 2007) (Figure 1A). FcR-mediated phagocytosis efficiency was then measured after incubation of the cells with IgG-coated red blood cells (IgG-RBC). Silencing of Bcl10 impaired phagocytosis, whereas its overexpression led to higher phagocytosis efficiency than in control cells (Figure 1D). The overexpression of FLAG-S138A, previously shown to inhibit TCR-mediated actin remodeling (Rueda et al., 2007), strongly inhibited FcR-induced phagocytosis. In addition, the absence of Bcl10 in primary human monocyte-derived macrophages (MDM) treated with siRNA (Figures 1B and 1E) and in macrophages derived from bone marrows (BMDM) of Bcl10 knockout ($Bcl10^{-/-}$) (Ruland et al., 2001) mice (Figures 1C and 1F) also led to inhibition of FcR-mediated phagocytosis, whereas initial binding of the particles was not affected.

These results demonstrate that Bcl10 contributes to FcR-mediated phagocytosis in human and mouse monocytes/macrophages.

We next analyzed in more detail the phagocytosis defect observed. Bcl10 KD cells or control cells were incubated with IgG-RBC for different time points, then fixed, and stained for external and internal RBC and F-actin. The number of F-actin-enriched phagocytic cups present at the surface of the cells and the number of internalized RBC were quantified for each time point. Control cells exhibited a peak of actin cup formation at 2 min that progressively decreased until 10 min, corresponding to the internalization of the RBC (Figures 1G and 1H). Bcl10 KD cells displayed similar numbers of F-actin cups at 2 min, but 56% ± 9% of the originally formed cups stayed opened and were still observable at the cell surface at 10 min. Those cups finally collapsed, resulting in a strong defect in internalization efficiency at 30 min. A similar defect was observed in $Bcl10^{-/-}$ BMDM, which was even more pronounced that actin cup formation was initiated as early as 30 s after contact in wild-type BMDM (Figures 1I and S1 available online).

Quantification of the fluorescence intensity associated with F-actin staining in phagocytic cups compared to the cortical area of the cell indicated similar amounts of F-actin in cups formed at 5 min in Bcl10 KD and control cells (Figures 1J and 1K). However, the aborted cups that remained for 10 min at the surface of the Bcl10 KD cells showed an increase in F-actin content compared to control cups or cups formed at 5 min in Bcl10 KD cells, suggesting that F-actin polymerization activity persisted and actin filaments accumulated (Figure 1K). Moreover, these blocked cups exhibited a different morphology by fluorescence microscopy (Figure 1H), which was further examined by scanning electron microscopy (Figure 1L). Unlike the cups observed in control cells at 5 min, which displayed thin membrane extensions tightly apposed against the particle, the Bcl10 KD cups exhibited disorganized and shorter extensions around the RBC both at 5 and 10 min. As observed by fluorescence microscopy, particles were internalized in control cells at 10 min (Figure 1L).

Together, these results indicate that Bcl10 is not required for the onset of actin polymerization but is rather critical for regulating phagocytic cup extension and closure.

The NFκB Complex Is Recruited but Not Required for Phagocytic Cup Formation

To further examine the link between the CBM signaling pathway and the role of Bcl10 in phagocytic cup formation, we analyzed the formation of the CBM complex upon FcR stimulation. We

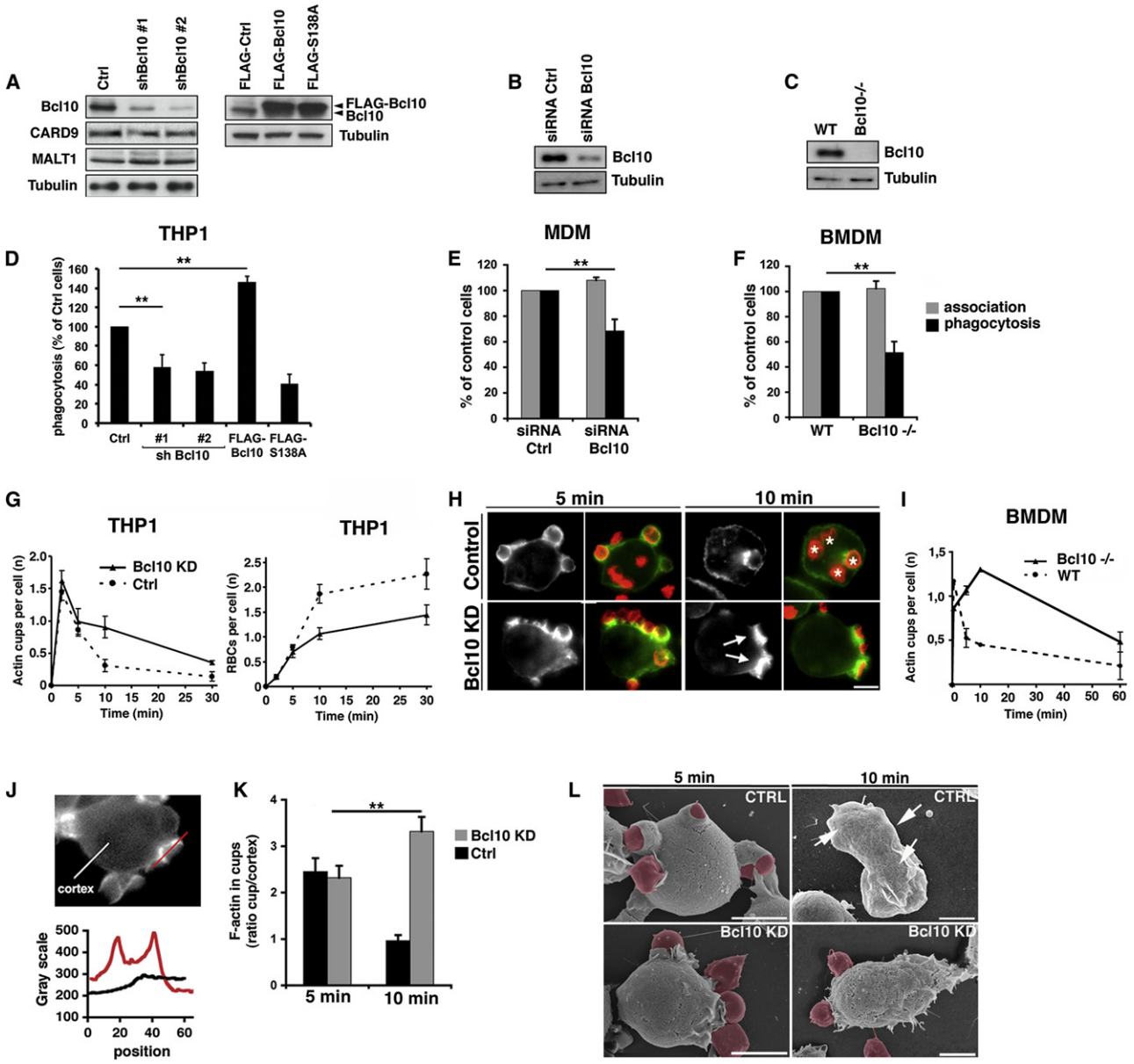

Figure 1. Bcl10 Promotes Phagocytic Cup Extension and Closure

(A) Immunoblot of lysates from THP1 cells stably transduced, either with control or two different shRNA sequences targeting Bcl10 (shRNA#1 and shRNA#2) (left), or transduced with plasmids encoding FLAG-tagged WT Bcl10 (FLAG-Bcl10) and its serine 138-to alanine mutant (FLAG-S138A) (right). Bcl10, CARD9, and Malt1 expression was analyzed using specific antibodies. Tubulin was used as a loading control.

(B and C) Immunoblots of lysates from human monocyte-derived macrophages (MDM) treated with control siRNA or siRNA-targeting Bcl10 (B) and bone-marrow-derived macrophages (BMDM) from WT mice or mice knockout for Bcl10 (Bcl10$^{-/-}$) (C). Bcl10 expression was analyzed, and tubulin was used as a loading control.

(D) Bcl10 knockdown cells (Bcl10 KD) with shRNA#1 or shRNA#2, as well as THP1 overexpressing FLAG-Bcl10 or FLAG-S138A were incubated with IgG-opsonized RBC (IgG-RBC) for 10 min and the phagocytosis efficiency was quantified in at least 50 cells per experiment. The results are expressed as the percentage of control cells ± SEM (n = 3 experiments, $p < 0.05$).

(E and F) Control MDM or MDM silenced for Bcl10 (E) and WT or Bcl10$^{-/-}$ BMDM (F) were incubated with IgG-RBC for 60 min and the RBC association efficiency (gray bars) and phagocytic activity (black bars) was quantified in at least 25 cells per experiment. The results are expressed as the percentage of control cells ± SEM (n = 3 experiments, $p < 0.05$).

(G) Bcl10 KD and control THP1 cells were incubated with IgG-RBC for the indicated times, and the number of F-actin-positive phagocytic cups per cell (left) and the corresponding number of internalized RBC (right) were quantified for at least 50 cells per experiment (data show the means ± SEM, n = 3).

(H) Control and Bcl10 KD cells were incubated with IgG-RBC for 5 or 10 min, fixed and labeled for F-actin (green) and IgG-RBC (red). Asterisks indicate internalized RBCs in control cells (upper panels) and arrows show open phagocytic cups with external RBC in Bcl10KD cells (lower panels) at 10 min. Scale bars, 5 μm.

(I) WT or Bcl10$^{-/-}$ BMDM were incubated with IgG-RBC for the indicated times and the mean number of F-actin-positive phagocytic cups per cell was quantified for at least 25 cells per experiment (data show the means ± SEM, n = 3).

incubated FLAG-Bcl10-expressing THP1 cells with IgG-RBC (or nonopsonized RBC as control) for 5 min in order to trigger FcR signaling and then immunoprecipitated Bcl10 (Figure 2). Malt1 was coimmunoprecipitated with FLAG-Bcl10 independently of FcR stimulation, confirming a previously described constitutive association between the two proteins (Uren et al., 2000), although a slight increase in binding was triggered by phagocytosis. In contrast, CARD9 association with Bcl10 was greatly enhanced upon phagocytosis (Figure 2A). The Ser138A mutant of Bcl10 showed a strong constitutive association with Malt1 and CARD9, which was not modified by phagocytosis. We next analyzed the localization of the CBM proteins during FcR-mediated phagocytosis in THP1 monocytes and in human primary macrophages by immunofluorescence. Bcl10, MALT1, and CARD9 were all recruited in phagocytic cups defined by the accumulation of F-actin (Figure 2B). In immune cells, the formation and activation of the CBM complex triggers the activation of the IKK complex, leading to the phosphorylation and degradation of IκBα, thus activating NFκB RelA/p50 dimers. We therefore analyzed whether the phagocytic cup could serve as a local and transient signaling platform that initiates the activation of the NF-κB pathway during the early steps of phagocytosis. Indeed, although nuclear translocation of RelA was observed only upon prolonged stimulation as expected (Figure 2E), both IκBα and RelA were found highly enriched at the site of phagocytosis after FcR stimulation in THP1 monocytes (Figure 2C), in primary mouse macrophages (Figure 2D), and in primary human macrophages (Figure 2E). In contrast, in the blocked cups formed at the surface of cells silenced or knockout for Bcl10, both RelA and IκBα exhibited a diffuse localization, which was not concentrated in the cortical area beneath the bound particle (Figures 2C and 2D). Thus, Bcl10 is critical to recruit the IKK complex at sites of phagosome formation, where the CBM complex is assembled and activated.

To further decipher the role of Bcl10 in activating IKK and NF-κB during phagocytosis, we analyzed the phosphorylation status of the IκBα regulatory subunit. Induction of phagocytosis led to an early and transient phosphorylation of IκBα correlating with the phagocytic cup closure step (5 and 10 min). Bcl10 silencing completely impaired IκBα phosphorylation, whereas overexpression of Bcl10 accelerated and increased its phosphorylation (Figure 2F). The overexpression of the S138A mutant of Bcl10, which perturbs actin polymerization but not IKK activation in T cells (Rueda et al., 2007) and inhibited phagocytosis (Figure 1D), led to the phosphorylation of IκBα as efficiently as the wild-type Bcl10 (Figure 2F), confirming that signaling to actin polymerization is not required for IKK activation. Inversely, to further analyze whether IKK activation is necessary for phagocytic cup formation, THP1 cells were transiently transfected to express a dominant negative mutant of IκBα (DN-IκBα), which inhibits the phosphorylation of endogenous IκBα and subsequent NF-κB activation. We found that DN-IκBα-transfected cells displayed a normal FcR-mediated phagocytic activity (Figure 2G).

Together, these data reveal a dual role for Bcl10. On one hand, Bcl10 regulates the recruitment and activation of the IKK complex and NF-κB at phagocytic sites. On the other hand, Bcl10 is able to modulate actin cytoskeleton dynamics, allowing closure of the phagocytic cup, which we decided to characterize in more details.

Silencing of Bcl10 Impairs Rac1 Activation

Because the stalled phagocytic cups present in Bcl10 KD cells accumulated F-actin, we examined the localization of some upstream factors known to stimulate actin assembly/disassembly during phagosome formation, including the Rho-family GTPases Cdc42 and Rac1 (Niedergang and Chavrier, 2005; Swanson, 2008). Previous studies had shown that Cdc42 is activated early during pseudopod extension, recruiting the N-WASP/WASP actin nucleation promoting factors, which in turn stimulate the Arp2/3 complex to promote actin nucleation and polymerization (Flannagan et al., 2012; Swanson, 2008). Here, we found that Arp3, N-WASP, and Cdc42 accumulated in higher amounts in the blocked cups formed at 10 min in Bcl10 KD cells as compared to normal phagocytic cups in control cells (Figures 3A and 3B). In contrast, we did not monitor significant changes in Rac1 recruitment (data not shown). We then analyzed the Rac1 activation status during FcR-induced phagocytosis by GTP pull-down assays. In control cells, Rac1 showed a transient activation peak at 5 and 10 min, correlating with phagocytic cup closure. In contrast, Bcl10 silencing resulted in both a higher basal activation of Rac1 and a defect in Rac1 activation (Figures 3C and 3D).

We next investigated the effects of overexpressing constitutive active (Rac1V12-GFP) or inactive (Rac1N17-GFP) mutants of Rac1 on phagosome formation in control and Bcl10 KD cells. First, we observed that wild-type Rac1 (Rac1WT-GFP) was enriched at the base of the phagocytic cup in control cells (Figure 3E). As previously described (Caron and Hall, 1998; Massol et al., 1998), expression of Rac1N17 impaired phagosome formation in control cells (Figure 3F). No additive defect was observed in Bcl10 KD cells transfected with Rac1N17. Transfection of the constitutively active mutant Rac1V12 increased phagocytic efficiency monitored 10 min after IgG-RBC binding in control cells, but most importantly, fully rescued the phagocytic defect displayed by Bcl10 KD cells (Figures 3E and 3F). Taken together, these data indicate that Rac1 is a downstream effector of Bcl10 and acts in a common signaling pathway crucial to regulate phagosome extension and closure.

The stalled cups formed in Bcl10-silenced cells displayed a phenotype similar to the one observed upon PI3K inhibition,

(J) Control and Bcl10 KD THP1 cells were incubated with IgG-RBC for 5 or 10 min and the amount of F-actin present at the phagocytic cup was quantified by fluorescence microscopy. The profiles of F-actin fluorescence intensities along the lines drawn at the phagocytic site (red line) and at the cell cortex (white line) are shown (lower graph).

(K) The fluorescence intensities measured in the phagocytic cups were divided by the fluorescence intensities measured for cortical actin. This ratio defined the index of recruitment. The means ± SEM of three independent experiments are plotted ($n = 60$ actin cups per condition, $p < 0.05$).

(L) Control and Bcl10 KD cells were incubated with IgG-RBC for 5 and 10 min and then fixed and processed for scanning EM. The RBC are pseudo-colored in red. Arrows indicate sites of membrane deformation due to potentially internalized particles. Scale bars, 5 μm.

See also Figure S1.

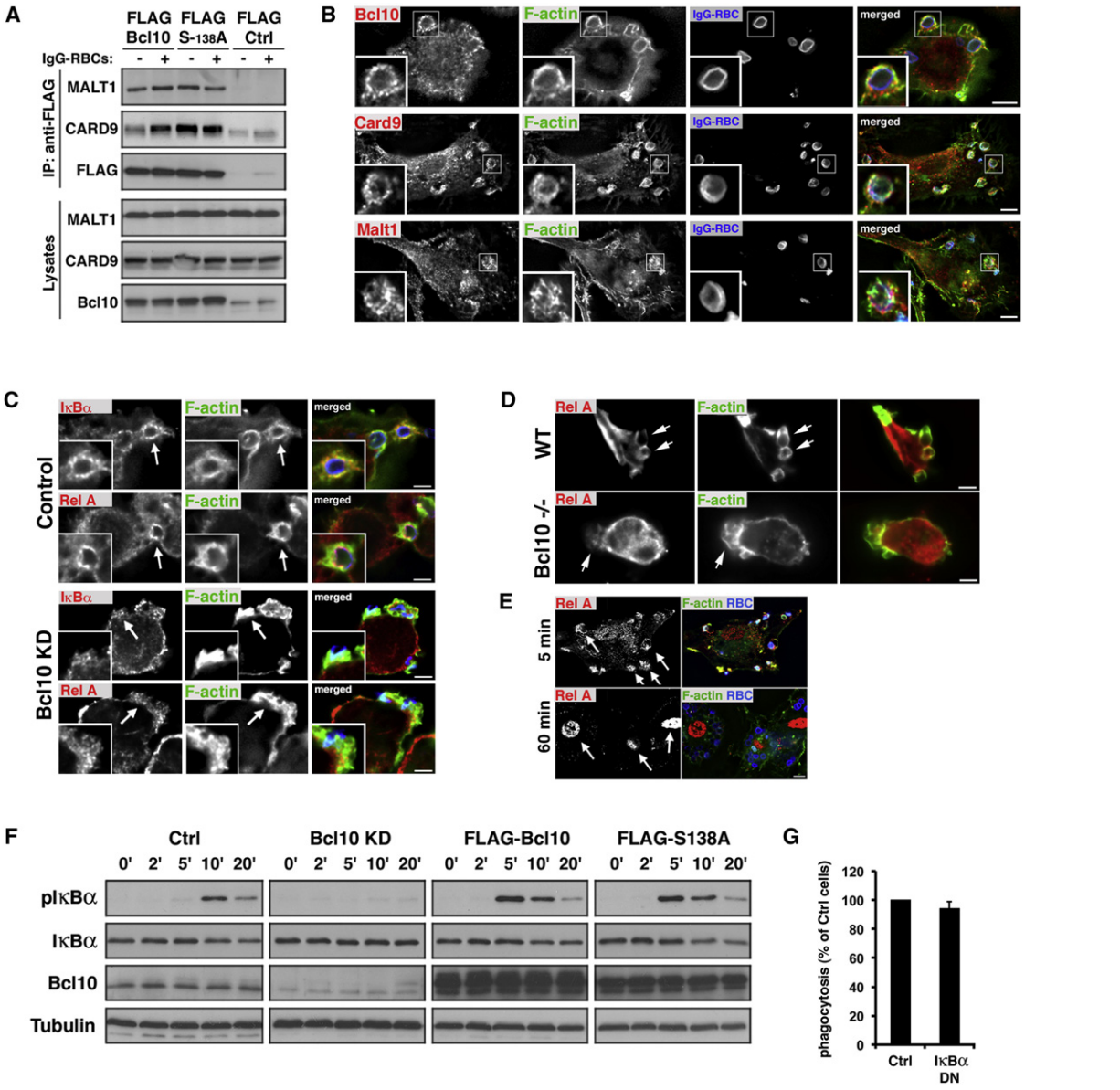

Figure 2. Bcl10 Triggers the Phagosome Recruitment and the Activation of the IκBα/NF-κB Pathway during Phagocytosis

(A) FLAG-Ctrl, FLAG-Bcl10, and FLAG-S138A cells were incubated with nonopsonized RBC (lane −) or IgG-RBC (lane +) for 5 min. FLAG-Bcl10 and FLAG-S138A were immunoprecipitated with anti-FLAG antibodies and coimmunoprecipitated endogenous CARD9 and Malt1 as revealed by specific antibodies (upper). The amounts of total proteins in lysates (5% of total lysate; lower panels) are shown in all conditions. FLAG-Ctrl cells were used as negative controls.

(B) FLAG-Bcl10-expressing THP1 cells or primary macrophages were incubated with IgG-RBC for 5 min, fixed, and labeled with anti-FLAG, anti-CARD9, or Malt1 (red) antibodies. F-actin in phagocytic cups was detected by incubation with phalloidin-Alexa488 (green). IgG-RBC were detected with secondary antibodies (blue). Scale bars, 5 μm.

(C) Control and Bcl10 KD THP1 cells were treated as in (B), and the localization of endogenous IκBα and RelA (red) was examined by immunofluorescence. Inserts show details of the phagocytic cup marked by an arrow. Scale bars, 5 μm.

(D) Detection of RelA (red) and F-actin (green) in WT or Bcl10$^{-/-}$ BMDM incubated with IgG-RBC for 5 min. Arrows indicate F-actin-positive phagocytic cups. Scale bars, 5 μm.

(E) Detection of RelA (red) in control MDM incubated with IgG-RBC for 5 min (upper panel) or 60 min (lower panel). F-actin (green) and RBC (blue) were also labeled. Arrows indicate RelA-positive phagocytic cups in the upper panel and RelA-positive nuclei in the lower panel. Bars: 5 μm.

(F) Ctrl, Bcl10 KD, FLAG-Bcl10, and FLAG-S138A cells were incubated with IgG-RBC for the indicated times. Cells were then lysed, and an equal amount of lysate was analyzed by western blot (WB) for phosphorylated IκBα (pIκBα), as well as total IκBα and Bcl10. Tubulin was used as a loading control.

(G) Control THP1 cells were transiently transfected for GFP as a negative control or dominant-negative IκBα (IκBα-DN), and phagocytosis efficiency was assessed by incubating cells with IgG-RBC for 30 min. The results are expressed as a percentage of control cells (mean ± SEM of three independent experiments, n = 30 cells per experiments).

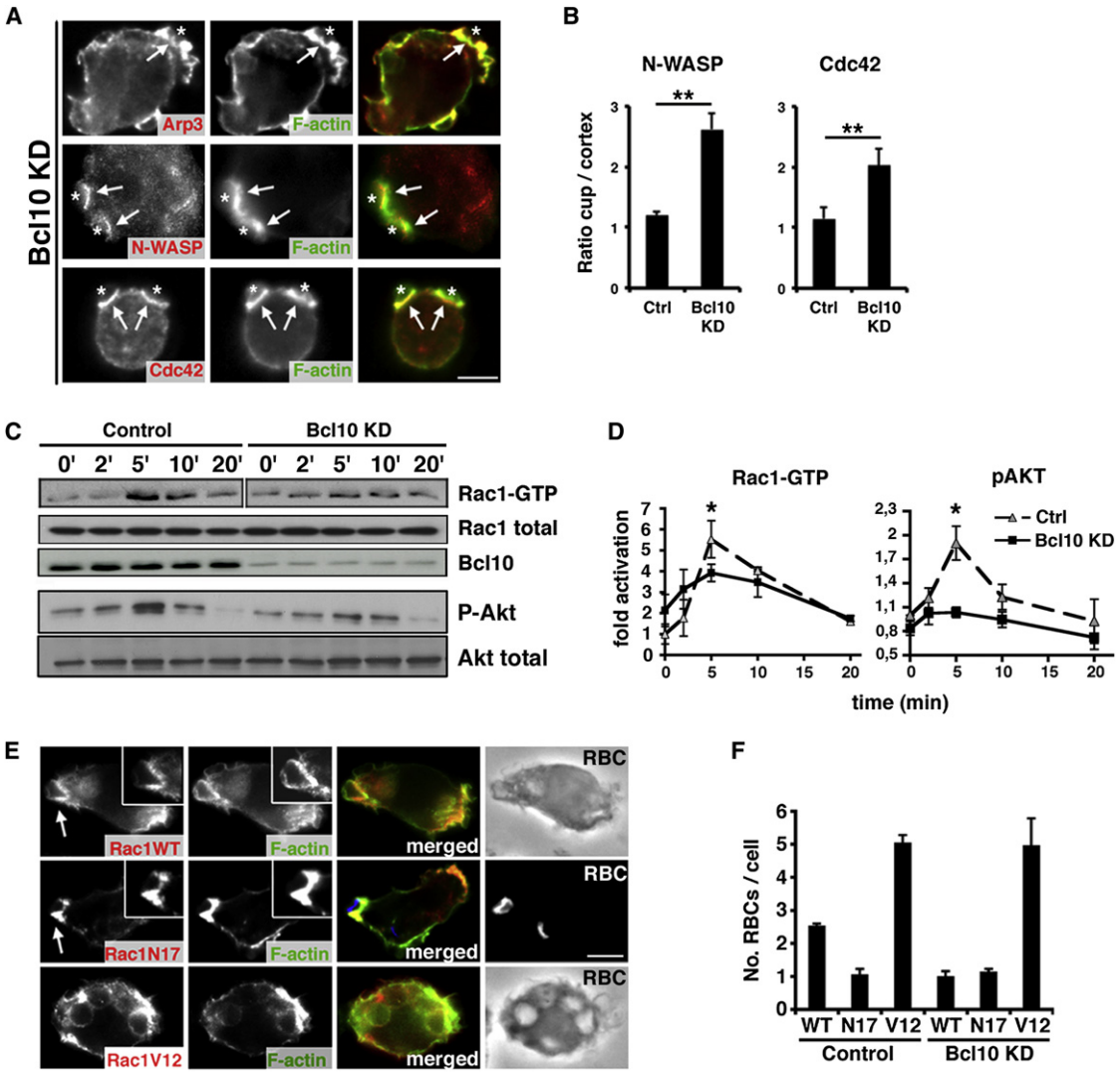

Figure 3. Silencing of Bcl10 Impairs Rac1 Activation

(A) Detection of Arp3, N-WASP, Cdc42 (red), and F-actin (green) in Bcl10 KD cells incubated with IgG-RBC for 10 min. Images show one z-plane of the cell analyzed by fluorescence microscopy. Scale bars, 5 μm.

(B) The recruitment of N-WASP and Cdc42 in phagocytic cups was quantified in Ctrl and Bcl10 KD cells by measuring the fluorescence intensities in the cups compared to the cortical region of the cell as described in Figures 1J and 1K. The means ± SEM of three independent experiments are plotted (n = 45 actin cups per condition, $p < 0.05$).

(C) Ctrl and Bcl10KD cells were incubated with IgG-RBC for the indicated times and lysed and an equal amount of total lysate was used to pull-down activated Rac1. The amount of Rac1-GTP in pull-down samples, and the amount of total Rac1 and Bcl10 in the lysates were analyzed by WB. Phosphorylated AKT (pAKT) and total AKT in the lysates were analyzed by WB (one representative experiment of three is shown).

(D) The graph indicates the fold activation of Rac1 (left) and AKT (right) induced upon phagocytosis, corresponding to the densitometric quantification of immunoblots as described in (C). Data show mean ± SEM from at least three independent experiments.

(E) Rac1WT-GFP, Rac1N17-GFP, and Rac1-V12 were transiently transfected in control THP1 cells, and their localization was analyzed by fluorescence microscopy (red) after incubation with IgG-RBC for 5 min (blue or phase contrast). F-actin was labeled in green. Scale bar, 5 μm.

(F) Quantification of the phagocytic efficiency (expressed as the mean number of RBC per cell ± SEM of three independent experiments, n = 40 cells per experiments) in Ctrl and Bcl10 KD cells transiently transfected with Rac1WT-GFP, Rac1N17-GFP, and Rac1-V12.

with accumulated Cdc42 and F-actin at the base of the cup and a defect in Rac1 activation (Araki et al., 1996). Therefore, PI3-K activation during phagocytosis in control and Bcl10 KD cells was examined by analyzing the phosphorylation status of Akt, a direct downstream effector of PI3-K. In control cells, Akt was transiently phosphorylated during phagosome formation with a maximal activation peak at 5 min. In Bcl10-silenced cells, Akt activation upon FcR stimulation was impaired (Figures 3C and 3D).

Altogether, the accumulation of F-actin and upstream effectors in the open Bcl10-deficient cups, and the correlating inhibition of Rac1 and PI3K in the absence of Bcl10, suggest that a specific transition signal involving Bcl10 is required to downregulate actin assembly, a step necessary for phagosome closure.

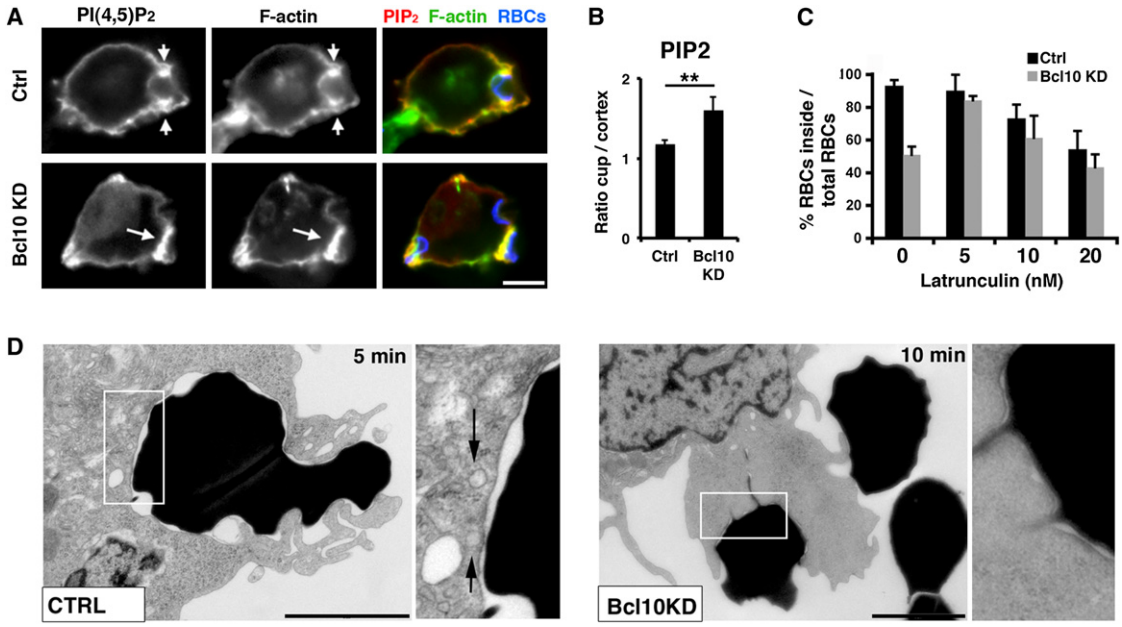

Figure 4. Actin Disassembly Is Sufficient to Rescue the Phagocytosis Defect in Bcl10 KD Cells

(A) The localization of PI(4,5)P_2 (red) was detected after transient transfection of Ctrl and Bcl10 KD THP1 cells to express the PH domain of PLCδ coupled to GFP. Cells were incubated with IgG-RBC for 5 and 10 min, respectively, fixed and stained for F-actin (green) and RBC (blue) and images were analyzed by fluorescence microscopy. Scale bars, 5 μm.

(B) Quantification of PI(4,5)P_2 recruitment in phagocytic cups in Ctrl and Bcl10 KD cells from images acquired as described in A ($p < 0.05$).

(C) Ctrl and Bcl10 KD cells were preincubated with the indicated amount of Latrunculin A for 30 min and phagocytosis was induced for 30 min. Phagocytic efficiency was quantified and expressed as the percentage of internalized RBC per cell/total amount of RBC detected. Data show the means ± SEM of three independent experiments (n = 45 cells per experiment).

(D) Transmission EM images of Ctrl and Bcl10KD cells incubated with IgG-RBC for 5 and 10 min, respectively, showing the distribution of intracellular vesicles around the phagocytic cups in each cell type. Scale bars, 2 μm.

Actin Disassembly Is Sufficient to Rescue the Phagocytosis Defect in Bcl10-Deficient Cells

Because Cdc42 inactivation and actin disassembly are dependent on PI(4,5)P_2 hydrolysis (Scott et al., 2005), we analyzed whether the accumulation of F-actin in the stalled phagocytic cups formed in Bcl10-silenced cells was correlated with an accumulation of PI(4,5)P_2. For this, the PH domain of PLCδ fused to GFP ($PH^{PLC\delta}$-GFP) was transiently expressed in control and Bcl10 KD cells. In control cells, we observed that PI(4,5)P_2 was preferentially enriched in the tips of pseudopods extending around the particle and almost absent from the base of the cup, as previously described (Scott et al., 2005). In contrast, in Bcl10 KD cells, PI(4,5)P_2 was found accumulated all around the blocked phagocytic cups, together with F-actin (Figures 4A and 4B). These results suggest that the absence of Bcl10 led to a defective PI(4,5)P_2 hydrolysis at the base of the phagocytic cup.

To directly investigate whether abnormal F-actin accumulation, likely caused by PI(4,5)P_2 accumulation, was the cause of the phagocytic defect, we treated Bcl10-depleted cells with very low amounts (5–20 nM) of the F-actin depolymerizing drug Latrunculin-A (LatA). In control cells, the addition of 5 nM LatA did not modify phagocytosis efficiency, whereas higher doses (10 and 20 nM) caused a decrease in phagocytosis (Figure 4C). Remarkably, phagocytic defects associated with Bcl10 depletion were completely rescued by 5 nM LatA treatment (Figure 4C). These observations show that abnormal F-actin levels are responsible for the defects in phagocytosis observed in the absence of Bcl10.

Finally, we examined by transmission electron microscopy the phagocytic cups formed in control and Bcl10 KD cells. Phagocytic cups in control cells displayed an actin-rich zone in the extending pseudopodia at 5 min, which were devoid of intracellular compartments. Intracellular vesicles were detected in the close vicinity of the plasma membrane in the region localized at the base of the nascent phagosome (Figure 4D). In contrast, blocked cups of Bcl10 KD cells exhibited a thick dense region all around the extending cup at 5 and 10 min, which was devoid of intracellular organelles (Figure 4D). This result suggests that the accumulation of F-actin in Bcl10-deficient phagocytic cups could be accompanied by a defect in focal delivery of vesicles, thereby impairing efficient phagosome formation.

Depolymerization of F-Actin and Focal Delivery of Intracellular Vesicles at the Base of the Forming Phagosome

The relative spatiotemporal localization of polymerizing actin and the delivery of intracellular compartments during phagosome formation has not been precisely investigated so far. To gain insight into this issue, we used the "frustrated phagocytosis" experimental setup, in which cells are allowed to spread on IgG-coated coverslips, combined with total internal reflexion

fluorescence microscopy (TIRFM) imaging to analyze the dynamic events taking place close to the plasma membrane (Figure 5A). RAW264.7 macrophages were transfected to transiently express VAMP3-GFP to label the endocytic compartments and Lifeact-mCherry to detect F-actin. The actin polymerization signal was clearly detected as an intense ring in the peripheral region of the spreading cell (Figure 5B; Movie S1). The lack of signal in the cell center was not due to a loss of cell adhesion because a GFP farnesylated construct, which targets the plasma membrane, was present in that region (data not shown). In contrast, VAMP3 was detected as punctuate dynamic structures in the central region of the cell, which was devoid of F-actin (Figure 5B). We designed a custom analysis with the ImageJ software and quantified that 67.9% ± 2.1% of the total VAMP3 vesicles were detected in the region (R2) defined as the cell center, whereas 32.1% were detected in the region R1, corresponding to the cell periphery, at sites of more intense F-actin staining (n = 5, Figures 5C and 5D). Cell spreading occurred in a completely disorganized manner on naked glass or on coverslips coated with polylysine (Figure S2). In that case, F-actin and VAMP3 staining were evenly distributed close to the plasma membrane. Therefore, the differential localization of F-actin and VAMP3 was specifically induced upon FcR triggering.

To get better insight into the three-dimensional (3D) spatiotemporal localization of endocytic compartments relative to actin polymerization during phagosome formation, we designed a specific "phagosome closure assay" to follow phagocytic cup extension and closure based on TIRFM. We coated glass coverslips with opsonized particles and observed the closure of the plasma membrane around the particles. This experimental setup enabled us to acquire TIRFM images of the tips of the pseudopods that are apposed to the glass coverslip and to concomitantly acquire the epifluorescence images at 3 μm distance above the coverslip (Figure 5E). We observed a clear recruitment of F-actin at the very tips of the closing pseudopods, whereas no VAMP3-positive vesicles could be detected in this closing zone of the phagocytic cup. VAMP3 was only detected as a diffuse signal corresponding to the plasma membrane (Figure 5F). In contrast, VAMP3-positive vesicles were clearly detected at the base of the nascent phagosome, only observed in the epifluorescence images (Figure 5F).

Together, our results clearly show that F-actin polymerization occurs in the tips of the extending pseudopods and that vesicular trafficking is localized at the base of the phagocytic cup in a zone where F-actin is depolymerized.

Bcl10 Controls Vesicular Trafficking at the Site of Phagocytosis

To get further insight into the molecular links between Bcl10 and the defective actin reorganization at sites of phagocytosis, we performed coimmunoprecipitation experiments with an anti-Bcl10 antibody and mass spectrometry analysis on lysates from THP1 monocytes. Unexpectedly, we found that AP1 and EpsinR were part of the proteins coimmunoprecipitated with Bcl10. We confirmed this result by western blot (Figure 6A). The same proteins were found immunoprecipitated with FLAG-Bcl10 using an anti-FLAG antibody in the FLAG-Bcl10-overexpressing cells (Figure 6B). Interestingly, AP1 and EpsinR were shown to interact and regulate transport between early endosomes and the *trans*-Golgi network (TGN) (Hirst et al., 2003; Popoff et al., 2007; Shiba et al., 2010). Furthermore, we previously described that AP1 is recruited to nascent phagosomes and required for efficient phagocytic cup formation in macrophages (Braun et al., 2007). Therefore, we first investigated whether EpsinR, like AP1, is functionally involved in FcR phagocytosis (Figure 6C). EpsinR depletion in control THP1 cells caused a 66% ± 18% decrease in phagocytic efficiency (Figure 6D), without any effect on particle binding, indicating a role of EpsinR in phagosome formation. We next analyzed the recruitment of AP1 and EpsinR at sites of phagosome formation. Although both proteins were found enriched in nascent phagosomes in control cells, their recruitment was strongly inhibited in the absence of Bcl10 (Figures 6E and 6F).

Our findings suggest that Bcl10 is required for the recruitment of AP1/EpsinR-positive endosomal compartments at sites of phagocytosis.

The OCRL PI(4,5)P_2 Phosphatase Is Recruited Downstream of Bcl10

Because Bcl10 was associated with the endocytic machinery and because PI(4,5)P_2 and F-actin accumulated in high amounts in Bcl10 KD cups, we decided to investigate the role of the PI(4,5)P_2 and PI(3,4,5)P_3 5-phosphatase OCRL, which is localized in cells in the TGN and peripheral endosomes (Choudhury et al., 2005; Erdmann et al., 2007), as it has been described for the proteins AP1 and EpsinR (Hirst et al., 2003). We therefore examined the colocalization of OCRL and AP1 in the whole cell and during phagocytosis in THP1 cells. As expected, we observed that OCRL and AP1 displayed a partial colocalization at the TGN level and in peripheral endosomes in nonstimulated cells (Figure S3). Most importantly, upon FcR stimulation, the two proteins were found colocalized in vesicles recruited at the phagocytic cup (Figure 6G, arrows). This observation suggests that OCRL could be delivered at sites of phagocytosis via the recruitment of AP1-positive compartments, which might play an essential role to regulate actin depolymerization, a step necessary for the completion of phagosome closure.

It has been recently shown that OCRL depletion causes a PI(4,5)P_2 and F-actin accumulation at the cleavage furrow of dividing cells, thereby impairing cytokinesis (Dambournet et al., 2011). In addition, it was shown that OCRL is required for efficient phagocytosis in *Dictyostelium discoideum* and in macrophages (Bohdanowicz et al., 2012; Loovers et al., 2007). We observed that OCRL was clearly enriched in nascent phagosomes in control THP1 monocytes and in primary human macrophages (Figures 7A and 7C). Importantly, this recruitment was strongly impaired in Bcl10 KD cells (Figures 7A and 7B). Moreover, OCRL depletion by siRNA in THP1 cells (Figure 7D) impaired FcR-mediated phagocytosis (Figure 7E). Importantly, treatment of the OCRL-depleted cells with 5 nM of LatA fully rescued the phagocytic defect (Figure 7E), as previously observed in Bcl10 KD monocytes (Figure 4C). To assess the functional role of OCRL relative to Bcl10, we silenced OCRL expression in FLAG-Bcl10-overexpressing cells (Figure 7F). The depletion of OCRL abolished the increase of phagocytosis normally observed in these cells (Figure 7G), suggesting that OCRL acts downstream of Bcl10 and participates in a common signaling pathway that regulates phagosome formation. We

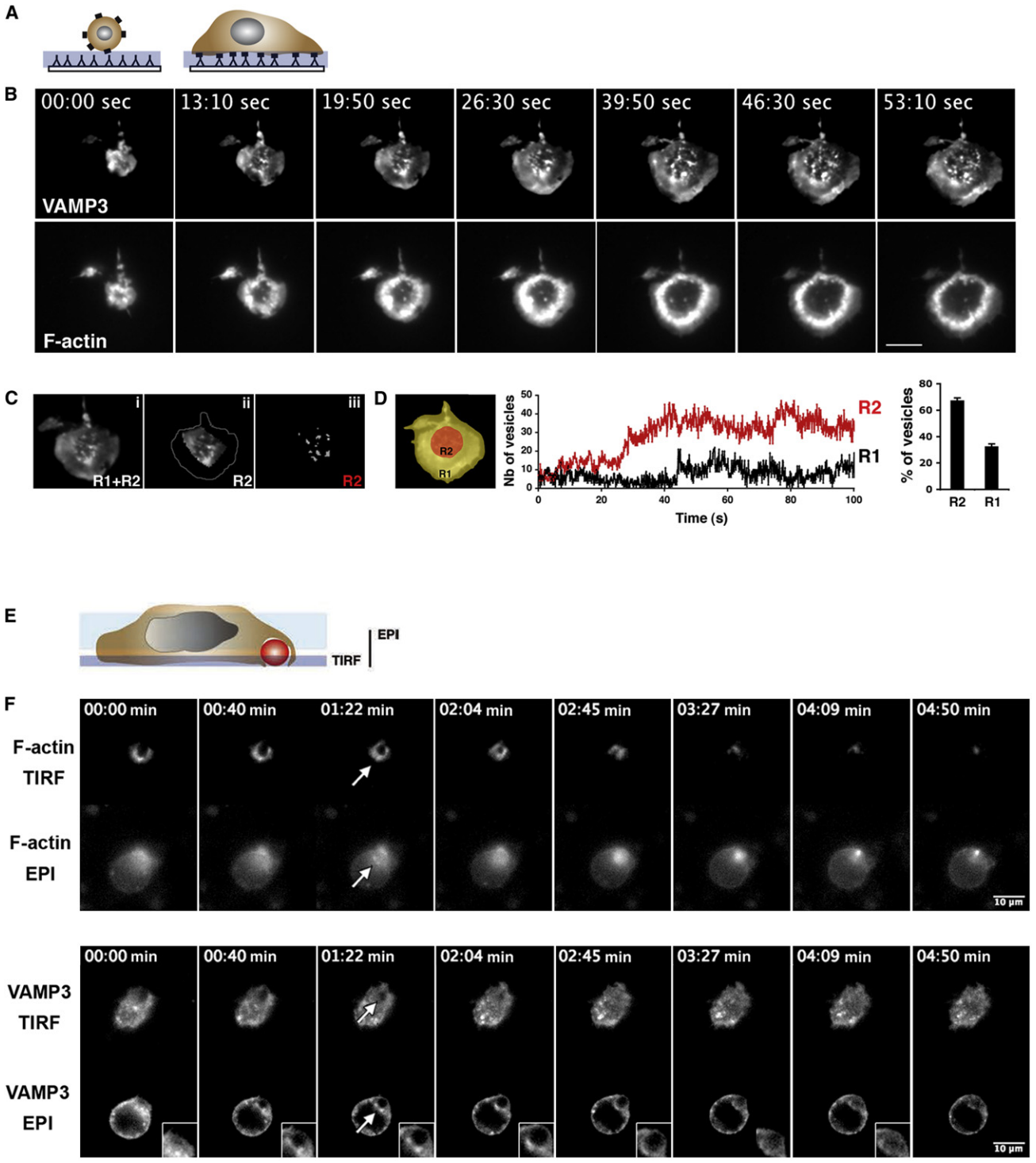

Figure 5. Spatiotemporal Organization of F-Actin and VAMP3 during Phagocytosis by Macrophages

(A) Schematic representation of the frustrated phagocytosis assay.

(B) Frustrated phagocytosis was performed using RAW264.7 murine macrophages transiently expressing Lifeact-mCherry and VAMP3-GFP. VAMP3-GFP (top) and Lifeact-mCherry (bottom) imaging by TIRFM were performed alternatively at 37°C every 100 ms during 120 s. Scale bar, 10 μm.

(C) Sequences of images illustrating the procedure used by the designed macrocommand in ImageJ software (see the Experimental Procedures); (1) total cell area (R1+R2); (2) R2 region obtained after 12 erosions; (3) TopHat filter detection of dotty particles in region R2.

(D) The number of VAMP3-positive vesicles was quantified and plotted over time in areas R2 and R1 corresponding respectively to the central region of the cell and to the cell periphery. The histogram on the right shows the mean percentage ± SEM of vesicles detected in the area R1 and R2 (n = 6 experiments).

(E) Schematic illustration of the phagosome closure assay.

finally analyzed by TIRFM the recruitment of OCRL-GFP-positive structures and actin polymerization events in the cortical region during frustrated phagocytosis (Figure 7H). In the majority of control cells, F-actin appeared enriched at the cell periphery and highly dynamic OCRL-positive structures were detected in the central region (9 out of 11 independent experiments). By contrast, in Bcl10 KD cells, polymerized actin was not localized in the cell periphery and OCRL-positive compartments were either very weakly detected in the TIRF region or appeared as immobile structures (in 5 out of 11 cases) (Figure 7H).

Together, our results suggest that the phagocytic defect observed in the absence of Bcl10 is due to the lack of recruitment of AP1 and OCRL-positive structures, which in turn causes local defects in actin remodeling.

DISCUSSION

Bcl10 is well known to contribute to the immune response by stimulating the activation of the IKK complex and NF-κB-mediated transcription of inflammatory genes downstream of antigen receptors in lymphocytes, and we found a similar function in macrophages. Unexpectedly, we observed that Bcl10 also mediated the active recruitment of IκBα and NF-κB to the membrane of the forming phagosome. This could serve to sequester the transcription factor before nuclear translocation, therefore allowing precise temporal and spatial control of the immune response. Interestingly, IκBα phosphorylation was not required for phagosome formation, suggesting that NF-κB activation and F-actin cytoskeleton remodeling are two independent functions exerted by Bcl10 during FcR phagocytosis in macrophages.

Here, we unraveled an original mechanism by which Bcl10 regulates phagocytic cup extension and closure. Using a dedicated assay based on TIRF microscopy, we analyzed the localization of F-actin and vesicular trafficking during phagocytic cup formation in 3D. We clearly observed that vesicular trafficking events were concentrated at the base of the phagocytic cup where actin was depolymerized. It remains possible that discrete and transient polymerization activities of the actin meshwork play a positive role in the fine-tuning of vesicles docking and exocytosis (Malacombe et al., 2006), but in the phagocytic cup, the mutual exclusion of actin and vesicles argues for a model in which actin filaments act as a barrier that blocks vesicle docking at the plasma membrane.

The phagocytic defect monitored in Bcl10 KD, as well as OCRL KD cells could be rescued by low doses of actin depolymerizing drugs, suggesting that actin depolymerization is indeed a prerequisite to complete phagosome closure. It was shown that Cdc42 inactivation and F-actin disappearance at the basis of the cup are directly correlated with and dependent on $PI(4,5)P_2$ hydrolysis (Scott et al., 2005). During phagosome formation, several pathways contribute to the disappearance of $PI(4,5)P_2$. Besides the arrest of its synthesis, PLCγ hydrolyzes $PI(4,5)P_2$. $PI(4,5)P_2$ is also phosphorylated and thereby consumed by PI3K into $PI(3,4,5)P_3$. Previous studies demonstrate that the accumulated 3′PIs provide a negative feedback response to deactivate Cdc42 that allows actin disassembly necessary for phagosome closure (Beemiller et al., 2010). In other systems, Rac1 and PI3K have been reported to signal in a positive feedback loop to sustain PI3K activity (Welch et al., 2003). Therefore, the defect in PI3K activity that we observed in Bcl10 silenced cells might be the consequence of a defect in Rac1 activation and, most importantly, could participate in the $PI(4,5)P_2$ consumption defect.

Additionally, $PI(4,5)P_2$ is hydrolyzed at the forming phagosome by 5-phosphoinositide phosphatases, such as inositol polyphosphate-5-phosphatase (Inpp5) and/or OCRL (Bohdanowicz et al., 2012). OCRL has been shown to be localized in the TGN and in peripheral endosomal structures, together with AP1 (Choudhury et al., 2005). We observed that Bcl10 silencing impaired AP1 and OCRL delivery to the phagocytic cup. Based on these findings, and because OCRL was reported to prefer $PI(4,5)P_2$ (Zhang et al., 1995), we propose that OCRL could locally participate to the hydrolysis of $PI(4,5)P_2$ and/or $PI(3,4,5)P_3$ to complete phagosome closure. Interestingly, recent data demonstrate that during *Yersinia* entry in macrophages, the fusion of Rab5-positive vesicles with the forming vacuole requires PI3K activity and that this event is essential for the recruitment of OCRL and Inpp5b and the subsequent hydrolysis of $PI(4,5)P_2$ (Sarantis et al., 2012). Consistent with these findings, our data indicate that Bcl10 is required for the stimulation of Rac1 and PI3K activity, as well as the recruitment of OCRL, which also binds to Rac1 via a Rho GAPlike domain, although the GAP activity was not shown in vivo (Faucherre et al., 2003). Both activities allow a rapid and efficient clearance of $PI(4,5)P_2$ in order to complete phagosome closure.

Here we found that Bcl10 interacts with AP1 and EpsinR. Importantly, we also performed Bcl10 pull-down experiments with lysates of T cells after TCR activation. By mass spectroscopy analysis, AP1 and AGAP2, a GAP factor for ARF1, were found specifically associated with Bcl10 after T cell stimulation (data not shown). We previously demonstrated that AP1 is recruited at phagocytic sites under the control of ARF1 (Braun et al., 2007). ARF1 activation is PI3K-dependent, and its inhibition impaired phagosome closure but not the initial step of pseudopod extension (Beemiller et al., 2006). Furthermore, it has been shown that AGAP2 is a $PI(4,5)P_2$-dependent ARF1GAP that associates with a fast recycling compartment containing AP1, Rab4, and the transferrin receptor (Nie et al., 2005). Therefore, it is conceivable that Bcl10 controls the activation status of ARF1, and thus the membrane association of AP1 and the endosomal dynamics that in turn regulate $PI(4,5)P_2$ hydrolysis and actin depolymerization. Presumably, factors other than OCRL are delivered to the phagocytic cup via the AP1-positive vesicles and a dynamic association/dissociation of signaling components is required for efficient actin

(F) RAW264.7 macrophages transiently expressed both Lifeact-mCherry and VAMP3-GFP. Lifeact-mCherry acquisitions (top) in TIRFM (top) and Epifluorescence (bottom), and VAMP3-GFP (bottom) in TIRFM (top) and Epifluorescence (bottom) imaging were performed alternatively at 37°C every 50 ms by switching from TIRF plan to RBC region (ΔZ = 3 μm) using a piezo. One region of interest is shown (arrows and inserts), corresponding to the phagocytic area for each epifluorescence picture. Scale bar, 10 μm.
See also Figure S2.

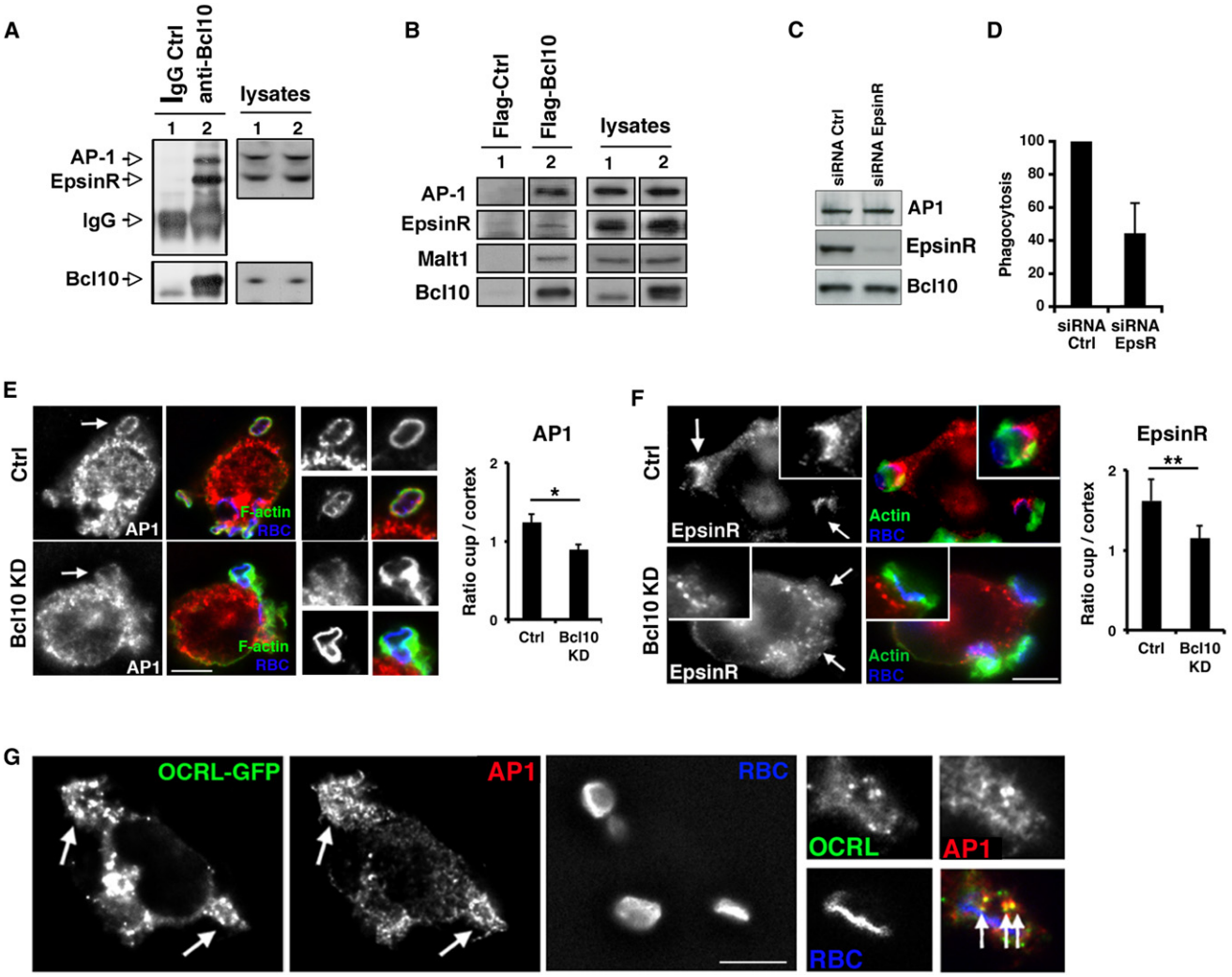

Figure 6. Bcl10 Regulates the Recruitment of AP1/EpsinR-Positive Compartments at the Site of Phagocytosis

(A) THP1 cell lysates were incubated with polyclonal anti-Bcl10 antibodies or irrelevant polyclonal IgG, and coimmunoprecipitated proteins were analyzed by WB. The amount of total proteins in lysates (5% of total lysate; right) are shown in all conditions.

(B) Lysates from FLAG or FLAG-Bcl10-expressing cells were incubated with monoclonal anti-FLAG antibodies, and coimmunoprecipitated proteins were analyzed by WB using anti-AP1, EpsinR, Bcl10, and Malt1 antibodies.

(C)THP1 cells were treated with siRNA control or siRNA-targeting EpsinR. Equal amount of lysates were analyzed by WB. Bcl10 was used as a loading control.

(D) Quantification of the phagocytic efficiency in EpsinR-silenced cells. The data are expressed as the percentage of control cells and show the mean ± SEM of three independent experiments.

(E and F) Immunofluorescence detection of AP1 (E) and EpsinR (F) in Ctrl and Bcl10 KD cells incubated with IgG-RBC (blue) for 5 and 10 min, respectively. F-actin is shown in green. Images represent one z-plane of the cell analyzed by fluorescence microscopy and deconvolution. The histogram on the right of each image panel indicates the quantification of AP1 (E) and EpsinR (F) recruitment in the phagocytic cups in Ctrl and Bcl10 KD cells, as described previously. Data show the means ± SEM of three independent experiments ($n = 75$ phagosomes, $p < 0.05$). Scale bars, 5 μm.

(G) Ctrl THP1 cells were transiently transfected with OCRL-GFP (green) and incubated with IgG-RBC (blue) for 5 min and colocalization with AP1 (red) was analyzed by immunofluorescence. Arrows indicate two different phagocytic cups. Inserts on the right represent a different z-plane of the cell and show details of the lower phagocytic cup. Arrows indicate vesicles detected at the cup, positive for OCRL (green) and AP1 (red). Scale bars, 5 μm.

See also Figures S3 and S4.

polymerization/depolymerization cycle. Indeed, the Ser138A mutant of Bcl10, which acts as a dominant negative mutant for phagocytosis, was found to be constitutively associated with CARD9 and AP1 (Figure S4). This appeared to efficiently block actin dynamics and pseudopod closure efficiently. Thus, our data argue for a model in which the vesicular delivery of intracellular compartments is not only a way to release plasma membrane tension but also allows to deliver signaling cargos that regulate F-actin dynamics and phagosome closure. We propose that intracellular compartments (AP1, EpsinR positive) are required to provide signaling components, such as OCRL, promoting $PI(4,5)P_2$ consumption and depolymerization of actin at the base of phagocytic cups. This would then allow subdomains of the compartments

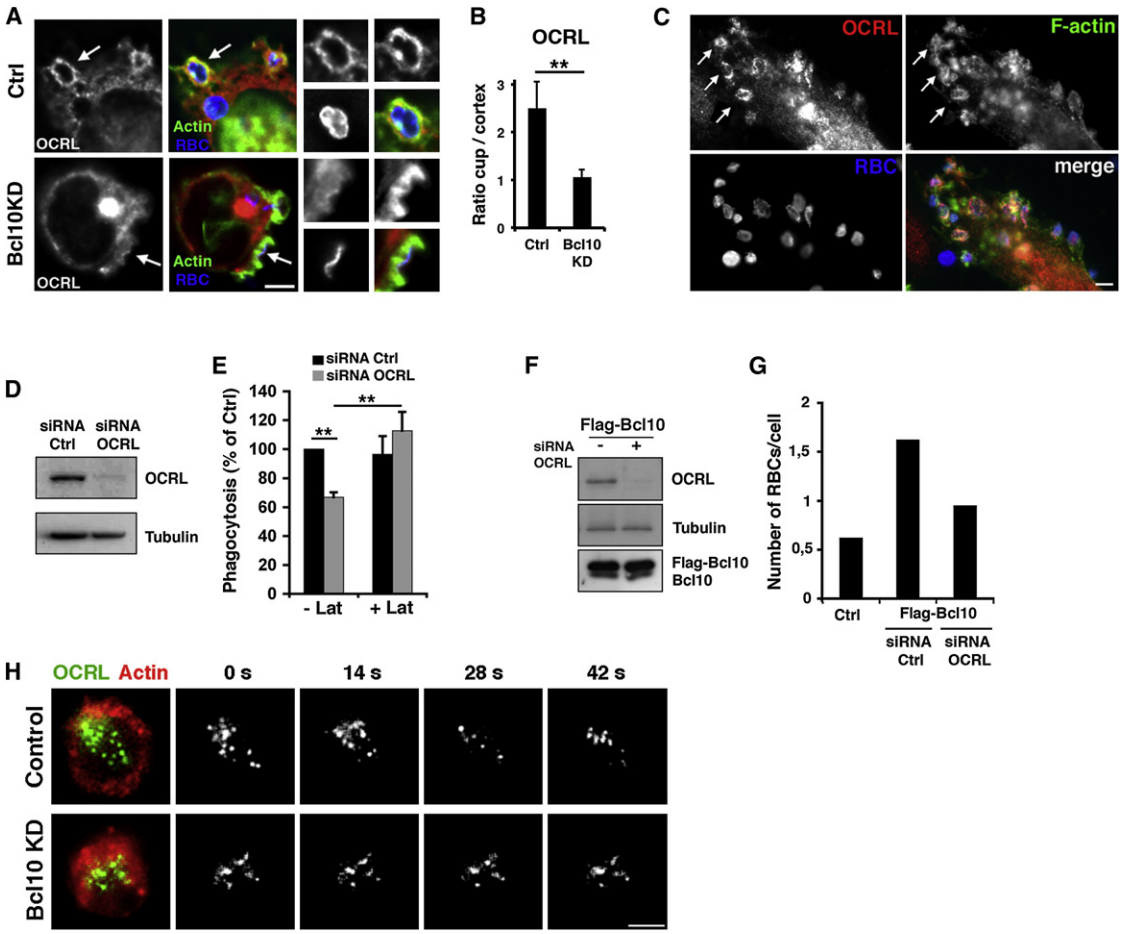

Figure 7. OCRL Is Recruited in Phagosomes Downstream of Bcl10

(A) Detection of endogenous OCRL (red) in Ctrl and Bcl10 KD cells incubated with IgG-RBC (blue) for 5 and 10 min, respectively. F-actin is shown in green. Images represent one z-plane of the cell analyzed by WF microscopy and deconvolved. Scale bars, 5 μm.

(B) The histogram indicates the quantification of OCRL recruitment in the phagocytic cups in Ctrl and Bcl10 KD cells, as described previously. Data show the means ± SEM of three independent experiments (n = 30 phagosomes per experiment, $p < 0.05$).

(C) Detection of endogenous OCRL (red) in primary human macrophages incubated with IgG-RBC (blue) for 5 min. F-actin was labeled in green. Scale bars, 2 μm.

(D) Immunoblots detecting OCRL from lysates of control THP1 cells transfected with control siRNA or targeting OCRL. Tubulin was used as a loading control.

(E) Quantification of phagocytic efficiency in THP1 cells treated with siRNA ctrl or siRNA OCRL, after incubation with IgG-RBC for 60 min, in absence (−Lat) or presence (+Lat) of 5 nM Latrunculin A. The results are expressed as the percentage of control cells ± SEM (n = 3 experiments, $p < 0.05$).

(F) Immunoblots detecting OCRL from lysates of FLAG-Bcl10 cells transfected with siRNA control (lane −) or targeting OCRL (lane +). Tubulin was used as a loading control.

(G) Quantification of phagocytic efficiency in FLAG-Bcl10 cells incubated with siRNA ctrl or OCRL, after incubation with IgG-RBC for 10 min. The data are expressed as the mean percentage of internalized RBC/total RBC from three independent experiments.

(H) Frustrated phagocytosis experiments were performed using transiently transfected Control (top) or Bcl10 KD (bottom) THP1 cells expressing both Lifeact-mCherry and OCRLA-GFP. OCRLA-GFP and Lifeact-mCherry imaging by TIRFM were performed alternatively at 37°C every 480 ms during 120 s. Sequences of images show the TIRF plan. Scale bar, 5 μm.

equipped with fusion machineries to bud and fuse with the plasma membrane (Braun et al., 2007; Niedergang et al., 2003), for further pseudopod extension.

In conclusion, we have unraveled an NF-κB-independent function for Bcl10 to promote intracellular trafficking and F-actin dynamics at the internalization step of phagocytosis. Emerging evidence indicates that Bcl10-containing signaling complexes are implicated downstream of a growing number of receptors, including not only immune receptors, but also EGFR or G-protein-coupled receptors (Rosebeck et al., 2011). Therefore, the Bcl10-dependent regulation of F-actin cytoskeleton and membrane trafficking that we observed in macrophages might be a mechanism involved in different functions in various cell types.

EXPERIMENTAL PROCEDURES

Information on antibodies, plasmids, cell culture, transfection and transduction, cell stimulation, immunoprecipitation and GST pull-down assays, transmission and scanning electron microscopy, and mass spectrometry are included in the Supplemental Experimental Procedures.

Phagocytosis Assay

Phagocytosis assays were performed with adherent cells plated on glass coverslips or with THP-1 cells plated onto poly-L-lysine-coated coverslips before incubation with IgG-opsonized SRBC (IgG-RBC) (Braun et al., 2004). For this, RBC were washed in PBS1X, incubated with anti-RBC antibodies for 30 minutes at room temperature (RT), then washed, and resuspended in serum-free medium. After internalization of the IgG-RBC for the indicated times, cells were fixed in 4% PFA/4% sucrose for 10 minutes, and external RBC were labeled for 10 minutes with Cy5-labeled F(ab')2 anti-mouse or anti-rabbit IgG in PBS/BSA 1%. Cells were then permeabilized with 0.05% saponine before labeling of the intracellular RBC with AMCA-labeled F(ab')2 anti-mouse or anti-rabbit IgG in PBS/saponine 0.05%/BSA 1%. To quantify phagocytosis, the ratio: number of internalized RBC/number of [internalized+ bound] RBC was calculated in at least 50 cells randomly chosen on the coverslips, corresponding to the phagocytic index. The index obtained was divided by the index obtained for control cells and expressed as a percentage of control cells. A minimum of three independent experiments was performed. We checked that control shRNA-depleted cells and parental nontransduced THP-1 cells showed similar phagocytosis efficiencies (data not shown). Immunofluorescence and image acquisition was performed on an inverted wide field microscope (Leica DMI6000, Leica Microsystems, Wetzlar, Germany) with a 100× (1.4 NA) objective and a MicroMAX Princeton Instruments). Z-series of images were taken at 0.2 μm increments, and deconvolution was performed with the software Huygens (Scientific Volume Imaging, Hilversum, The Netherlands). When indicated, images were acquired with an inverted spinning disk confocal microscope equipped with a CoolSnap HQ2 (Photometrics, Tucson, AZ, USA) camera.

Frustrated Phagocytosis Assay

Glass-bottom dishes of 35 mm in diameter (MatTek Corporation, El Segundo, CA, USA) were coated with anti-RBC IgG in PBS overnight at 4°C and then washed twice with PBS. Macrophages were resuspended in serum-free microscopy medium (red phenol-free RPMI 1640, 2 mM L-Glutamine, 10 mM HEPES, 1 mM sodium pyruvate, and 50 μM β-mercaptoethanol) and then allowed to sediment on the antibody-coated dishes at 37°C.

Phagosome Closure Assay

IgG-RBC was centrifuged onto 35 mm glass bottom dishes (MatTek Corporation) pretreated with 0.01% poly-L-Lysine in PBS for 30 minutes at RT. The dishes were then washed once with a 10% BSA in PBS solution and incubated with prewarmed serum-free microscopy medium. Macrophages were resuspended and allowed to sediment onto opsonized SRBC-coated dishes at 37°C.

Statistics

The statistical significance of the data was tested with an unpaired Student's t test. Differences were considered significant if p values were less than 0.05 (*) and 0.005 (**).

SUPPLEMENTAL INFORMATION

Supplemental information includes four figures, one movie, and Supplemental Experimental Procedures and can be found with this article online at http://dx.doi.org/10.1016/j.devcel.2012.09.021.

ACKNOWLEDGMENTS

We thank Andrés Alcover for his support; Benedicte Capron and Catherine Fabre (EFS Saint Vincent de Paul) for buffy coat supply; Jean-François Alkombre and his team (INRA, Center de Jouy-en-Josas) for collecting samples of sheep blood; the 3P5 Proteomic facility of Paris Descartes University for mass spectrometry; Céline Loussert and Antonio Mucciolo from the EM facility at the University of Lausanne; and Stéphanie Guadaginini from the EM facility at Pasteur Institute, Paris. This work was supported by grants from Fondation pour la Recherche Médicale (FRM, INE20041102865), CNRS (ATIP Program), Ville de Paris and Agence Nationale de la Recherche (ANR 2011-BSVSE3-025) to F.N. A.E. was supported by grants from Institut Pasteur, the CNRS, the Agence Nationale de la Recherche (ANR ANR07-JCJC-0089), and the Schlumberger Foundation for Education and Research. M.T. acknowledges support from the Swiss National Science Foundation and the Swiss Cancer League (Oncosuisse), as well as the foundations Leenaards, Pierre Mercier, and Novartis Consumer Health. S.M. was supported by postdoctoral fellowships from FRM and EMBO. J.M. was supported by a doctoral fellowship from ANRS.

Received: March 28, 2012
Revised: August 18, 2012
Accepted: September 21, 2012
Published online: November 12, 2012

REFERENCES

Araki, N., Johnson, M.T., and Swanson, J.A. (1996). A role for phosphoinositide 3-kinase in the completion of macropinocytosis and phagocytosis by macrophages. J. Cell Biol. *135*, 1249–1260.

Bajno, L., Peng, X.-R., Schreiber, A.D., Moore, H.-P., Trimble, W.S., and Grinstein, S. (2000). Focal exocytosis of VAMP3-containing vesicles at sites of phagosome formation. J. Cell Biol. *149*, 697–706.

Beemiller, P., Hoppe, A.D., and Swanson, J.A. (2006). A phosphatidylinositol-3-kinase-dependent signal transition regulates ARF1 and ARF6 during Fcgamma receptor-mediated phagocytosis. PLoS Biol. *4*, e162.

Beemiller, P., Zhang, Y., Mohan, S., Levinsohn, E., Gaeta, I., Hoppe, A.D., and Swanson, J.A. (2010). A Cdc42 activation cycle coordinated by PI 3-kinase during Fc receptor-mediated phagocytosis. Mol. Biol. Cell *21*, 470–480.

Bi, L., Gojestani, S., Wu, W., Hsu, Y.M., Zhu, J., Ariizumi, K., and Lin, X. (2010). CARD9 mediates dectin-2-induced IkappaBalpha kinase ubiquitination leading to activation of NF-kappaB in response to stimulation by the hyphal form of Candida albicans. J. Biol. Chem. *285*, 25969–25977.

Bohdanowicz, M., Balkin, D.M., De Camilli, P., and Grinstein, S. (2012). Recruitment of OCRL and Inpp5B to phagosomes by Rab5 and APPL1 depletes phosphoinositides and attenuates Akt signaling. Mol. Biol. Cell *23*, 176–187.

Braun, V., and Niedergang, F. (2006). Linking exocytosis and endocytosis during phagocytosis. Biol. Cell *98*, 195–201.

Braun, V., Fraisier, V., Raposo, G., Hurbain, I., Sibarita, J.B., Chavrier, P., Galli, T., and Niedergang, F. (2004). TI-VAMP/VAMP7 is required for optimal phagocytosis of opsonised particles in macrophages. EMBO J. *23*, 4166–4176.

Braun, V., Deschamps, C., Raposo, G., Benaroch, P., Benmerah, A., Chavrier, P., and Niedergang, F. (2007). AP-1 and ARF1 control endosomal dynamics at sites of FcR mediated phagocytosis. Mol. Biol. Cell *18*, 4921–4931.

Caron, E., and Hall, A. (1998). Identification of two distinct mechanisms of phagocytosis controlled by different Rho GTPases. Science *282*, 1717–1721.

Chen, Y., Pappu, B.P., Zeng, H., Xue, L., Morris, S.W., Lin, X., Wen, R., and Wang, D. (2007). B cell lymphoma 10 is essential for FcepsilonR-mediated degranulation and IL-6 production in mast cells. J. Immunol. *178*, 49–57.

Choudhury, R., Diao, A., Zhang, F., Eisenberg, E., Saint-Pol, A., Williams, C., Konstantakopoulos, A., Lucocq, J., Johannes, L., Rabouille, C., et al. (2005). Lowe syndrome protein OCRL1 interacts with clathrin and regulates protein trafficking between endosomes and the trans-Golgi network. Mol. Biol. Cell *16*, 3467–3479.

Dambournet, D., Machicoane, M., Chesneau, L., Sachse, M., Rocancourt, M., El Marjou, A., Formstecher, E., Salomon, R., Goud, B., and Echard, A. (2011). Rab35 GTPase and OCRL phosphatase remodel lipids and F-actin for successful cytokinesis. Nat. Cell Biol. *13*, 981–988.

Du, M.Q. (2007). MALT lymphoma : recent advances in aetiology and molecular genetics. J. Clin. Exp. Hematop. *47*, 31–42.

Erdmann, K.S., Mao, Y., McCrea, H.J., Zoncu, R., Lee, S., Paradise, S., Modregger, J., Biemesderfer, D., Toomre, D., and De Camilli, P. (2007). A role of the Lowe syndrome protein OCRL in early steps of the endocytic pathway. Dev. Cell *13*, 377–390.

Faucherre, A., Desbois, P., Satre, V., Lunardi, J., Dorseuil, O., and Gacon, G. (2003). Lowe syndrome protein OCRL1 interacts with Rac GTPase in the trans-Golgi network. Hum. Mol. Genet. *12*, 2449–2456.

Flannagan, R.S., Jaumouillé, V., and Grinstein, S. (2012). The cell biology of phagocytosis. Annu. Rev. Pathol. *7*, 61–98.

Goodridge, H.S., Shimada, T., Wolf, A.J., Hsu, Y.M., Becker, C.A., Lin, X., and Underhill, D.M. (2009). Differential use of CARD9 by dectin-1 in macrophages and dendritic cells. J. Immunol. *182*, 1146–1154.

Gross, O., Gewies, A., Finger, K., Schäfer, M., Sparwasser, T., Peschel, C., Förster, I., and Ruland, J. (2006). Card9 controls a non-TLR signalling pathway for innate anti-fungal immunity. Nature *442*, 651–656.

Häcker, H., and Karin, M. (2006). Regulation and function of IKK and IKK-related kinases. Sci. STKE *2006*, re13.

Hara, H., and Saito, T. (2009). CARD9 versus CARMA1 in innate and adaptive immunity. Trends Immunol. *30*, 234–242.

Hara, H., Ishihara, C., Takeuchi, A., Imanishi, T., Xue, L., Morris, S.W., Inui, M., Takai, T., Shibuya, A., Saijo, S., et al. (2007). The adaptor protein CARD9 is essential for the activation of myeloid cells through ITAM-associated and Toll-like receptors. Nat. Immunol. *8*, 619–629.

Hara, H., Ishihara, C., Takeuchi, A., Xue, L., Morris, S.W., Penninger, J.M., Yoshida, H., and Saito, T. (2008). Cell type-specific regulation of ITAM-mediated NF-kappaB activation by the adaptors, CARMA1 and CARD9. J. Immunol. *181*, 918–930.

Hirst, J., Motley, A., Harasaki, K., Peak Chew, S.Y., and Robinson, M.S. (2003). EpsinR: an ENTH domain-containing protein that interacts with AP-1. Mol. Biol. Cell *14*, 625–641.

Klemm, S., Gutermuth, J., Hültner, L., Sparwasser, T., Behrendt, H., Peschel, C., Mak, T.W., Jakob, T., and Ruland, J. (2006). The Bcl10-Malt1 complex segregates Fc epsilon RI-mediated nuclear factor kappa B activation and cytokine production from mast cell degranulation. J. Exp. Med. *203*, 337–347.

Loovers, H.M., Kortholt, A., de Groote, H., Whitty, L., Nussbaum, R.L., and van Haastert, P.J. (2007). Regulation of phagocytosis in Dictyostelium by the inositol 5-phosphatase OCRL homolog Dd5P4. Traffic *8*, 618–628.

Malacombe, M., Bader, M.F., and Gasman, S. (2006). Exocytosis in neuroendocrine cells: new tasks for actin. Biochim. Biophys. Acta *1763*, 1175–1183.

Massol, P., Montcourrier, P., Guillemot, J.-C., and Chavrier, P. (1998). Fc receptor-mediated phagocytosis requires CDC42 and Rac1. EMBO J. *17*, 6219–6229.

Ngo, V.N., Davis, R.E., Lamy, L., Yu, X., Zhao, H., Lenz, G., Lam, L.T., Dave, S., Yang, L., Powell, J., and Staudt, L.M. (2006). A loss-of-function RNA interference screen for molecular targets in cancer. Nature *441*, 106–110.

Nie, Z., Fei, J., Premont, R.T., and Randazzo, P.A. (2005). The Arf GAPs AGAP1 and AGAP2 distinguish between the adaptor protein complexes AP-1 and AP-3. J. Cell Sci. *118*, 3555–3566.

Niedergang, F., Colucci-Guyon, E., Dubois, T., Raposo, G., and Chavrier, P. (2003). ADP ribosylation factor 6 is activated and controls membrane delivery during phagocytosis in macrophages. J. Cell Biol. *161*, 1143–1150.

Niedergang, F., and Chavrier, P. (2005). Regulation of phagocytosis by Rho GTPases. Curr. Top. Microbiol. Immunol. *291*, 43–60.

Popoff, V., Mardones, G.A., Tenza, D., Rojas, R., Lamaze, C., Bonifacino, J.S., Raposo, G., and Johannes, L. (2007). The retromer complex and clathrin define an early endosomal retrograde exit site. J. Cell Sci. *120*, 2022–2031.

Rawlings, D.J., Sommer, K., and Moreno-García, M.E. (2006). The CARMA1 signalosome links the signalling machinery of adaptive and innate immunity in lymphocytes. Nat. Rev. Immunol. *6*, 799–812.

Rosebeck, S., Rehman, A.O., Lucas, P.C., and McAllister-Lucas, L.M. (2011). From MALT lymphoma to the CBM signalosome: three decades of discovery. Cell Cycle *10*, 2485–2496.

Rueda, D., Gaide, O., Ho, L., Lewkowicz, E., Niedergang, F., Hailfinger, S., Rebeaud, F., Guzzardi, M., Conne, B., Thelen, M., et al. (2007). Bcl10 controls TCR- and FcgammaR-induced actin polymerization. J. Immunol. *178*, 4373–4384.

Ruland, J., Duncan, G.S., Elia, A., del Barco Barrantes, I., Nguyen, L., Plyte, S., Millar, D.G., Bouchard, D., Wakeham, A., Ohashi, P.S., and Mak, T.W. (2001). Bcl10 is a positive regulator of antigen receptor-induced activation of NF-kappaB and neural tube closure. Cell *104*, 33–42.

Sarantis, H., Balkin, D.M., De Camilli, P., Isberg, R.R., Brumell, J.H., and Grinstein, S. (2012). Yersinia entry into host cells requires Rab5-dependent dephosphorylation of PI(4,5)P_2 and membrane scission. Cell Host Microbe *11*, 117–128.

Scott, C.C., Dobson, W., Botelho, R.J., Coady-Osberg, N., Chavrier, P., Knecht, D.A., Heath, C., Stahl, P., and Grinstein, S. (2005). Phosphatidylinositol-4,5-bisphosphate hydrolysis directs actin remodeling during phagocytosis. J. Cell Biol. *169*, 139–149.

Shiba, Y., Römer, W., Mardones, G.A., Burgos, P.V., Lamaze, C., and Johannes, L. (2010). AGAP2 regulates retrograde transport between early endosomes and the TGN. J. Cell Sci. *123*, 2381–2390.

Strasser, D., Neumann, K., Bergmann, H., Marakalala, M.J., Guler, R., Rojowska, A., Hopfner, K.P., Brombacher, F., Urlaub, H., Baier, G., et al. (2012). Syk kinase-coupled C-type lectin receptors engage protein kinase C-σ to elicit Card9 adaptor-mediated innate immunity. Immunity *36*, 32–42.

Swanson, J.A. (2008). Shaping cups into phagosomes and macropinosomes. Nat. Rev. Mol. Cell Biol. *9*, 639–649.

Thome, M., and Weil, R. (2007). Post-translational modifications regulate distinct functions of CARMA1 and BCL10. Trends Immunol. *28*, 281–288.

Thome, M., Charton, J.E., Pelzer, C., and Hailfinger, S. (2010). Antigen receptor signaling to NF-kappaB via CARMA1, BCL10, and MALT1. Cold Spring Harb. Perspect. Biol. *2*, a003004.

Touret, N., Paroutis, P., and Grinstein, S. (2005). The nature of the phagosomal membrane: endoplasmic reticulum versus plasmalemma. J. Leukoc. Biol. *77*, 878–885.

Uren, A.G., O'Rourke, K., Aravind, L.A., Pisabarro, M.T., Seshagiri, S., Koonin, E.V., and Dixit, V.M. (2000). Identification of paracaspases and metacaspases: two ancient families of caspase-like proteins, one of which plays a key role in MALT lymphoma. Mol. Cell *6*, 961–967.

Welch, H.C., Coadwell, W.J., Stephens, L.R., and Hawkins, P.T. (2003). Phosphoinositide 3-kinase-dependent activation of Rac. FEBS Lett. *546*, 93–97.

Wu, W., Hsu, Y.M., Bi, L., Songyang, Z., and Lin, X. (2009). CARD9 facilitates microbe-elicited production of reactive oxygen species by regulating the LyGDI-Rac1 complex. Nat. Immunol. *10*, 1208–1214.

Xue, L., Morris, S.W., Orihuela, C., Tuomanen, E., Cui, X., Wen, R., and Wang, D. (2003). Defective development and function of Bcl10-deficient follicular, marginal zone and B1 B cells. Nat. Immunol. *4*, 857–865.

Zhang, X., Jefferson, A.B., Auethavekiat, V., and Majerus, P.W. (1995). The protein deficient in Lowe syndrome is a phosphatidylinositol-4,5-bisphosphate 5-phosphatase. Proc. Natl. Acad. Sci. USA *92*, 4853–4856.